1-1-2019

Low-Coordinate Iridium Oxide Confined on Graphitic Carbon Nitride for Highly Efficient Oxygen Evolution

Jiayi Chen
University of Wollongong, jc309@uowmail.edu.au

Peixin Cui
Chinese Academy Of Sciences

Guoqiang Zhao
University of Wollongong, gz815@uowmail.edu.au

Kun Rui
University of Wollongong, krui@uow.edu.au

Mengmeng Lao
University of Wollongong, ml590@uowmail.edu.au

See next page for additional authors

Low-Coordinate Iridium Oxide Confined on Graphitic Carbon Nitride for Highly Efficient Oxygen Evolution

Abstract

Highly active and durable electrocatalysts for the oxygen evolution reaction (OER) is greatly desired. Iridium oxide/graphitic carbon nitride (IrO_2/GCN) heterostructures are designed with low-coordinate IrO_2 nanoparticles (NPs) confined on superhydrophilic highly stable GCN nanosheets for efficient acidic OER. The GCN nanosheets not only ensure the homogeneous distribution and confinement of IrO_2 NPs but also endows the heterostructured catalyst system with a superhydrophilic surface, which can maximize the exposure of active sites and promotes mass diffusion. The coordination number of Ir atoms is decreased owing to the strong interaction between IrO_2 and GCN, leading to lattice strain and increment of electron density around Ir sites and hence modulating the attachment between the catalyst and reaction intermediates. The optimized IrO_2/GCN heterostructure delivers not only by far the highest mass activity among the reported IrO_2-based catalysts but also decent durability.

Disciplines

Engineering | Physical Sciences and Mathematics

Publication Details

Chen, J., Cui, P., Zhao, G., Rui, K., Lao, M., Chen, Y., Zheng, X., Jiang, Y., Pan, H., Dou, S. Xue. & Sun, W. (2019). Low-Coordinate Iridium Oxide Confined on Graphitic Carbon Nitride for Highly Efficient Oxygen Evolution. Angewandte Chemie - International Edition, 58 (36), 12540-12544.

Authors

Jiayi Chen, Peixin Cui, Guoqiang Zhao, Kun Rui, Mengmeng Lao, Yaping Chen, Xusheng Zheng, Yinzhu Jiang, Hongge Pan, Shi Xue Dou, and Wenping Sun

COMMUNICATION

Low-Coordinate Iridium Oxide Confined on Graphitic Carbon Nitride for Highly Efficient Oxygen Evolution

Jiayi Chen[+], Peixin Cui[+], Guoqiang Zhao[+], Kun Rui, Mengmeng Lao, Yaping Chen, Xusheng Zheng,* Yinzhu Jiang, Hongge Pan, Shi Xue Dou, and Wenping Sun*

This work is dedicated to Prof. S. X. Dou on the occasion of his 80th birthday.

Abstract: Developing highly active and durable electrocatalysts for oxygen evolution reaction (OER) is greatly desired for efficient water electrolyzers. Herein, new iridium oxide/graphitic carbon nitride (IrO_2/GCN) heterostructures are designed with low-coordinated IrO_2 nanoparticles (NPs) confined on superhydrophilic and highly stable GCN nanosheets toward efficient acidic OER. The multifunctional GCN nanosheets not only ensure the homogeneous distribution and confinement of IrO_2 NPs but also endows the heterostructured catalyst system with a superhydrophilic surface, which can significantly maximize the exposure of active sites and promotes mass diffusion, respectively. The coordination number of Ir atoms is decreased due to the strong interaction between IrO_2 and GCN, leading to lattice strain and increment of electron density around Ir sites and hence modulating the attachment between the catalyst and reaction intermediates. The optimized IrO_2/GCN heterostructure delivers not only by far the highest mass activity among the reported IrO_2-based catalysts but also decent durability.

Contrary to the rapid development of renewable energies harvesting technologies, the utilization efficiency of renewable energies is far from satisfaction due to their intermittent nature. Electrochemical water splitting driven by renewable electricity is a practical strategy to solve this problem.[1] Proton exchange membrane water electrolyzers (PEMWEs), which operate water electrolysis in acidic media, show great advantages over alkaline electrolyzers.[2] One major challenge for PEMWEs is developing highly efficient electrocatalysts for acidic oxygen evolution reaction (OER). Specifically, the harsh working environment of acidic OER requires the catalysts possessing extremely high chemical stability against corrosion and oxidation.[2] To date, iridium-based catalysts are the only choice for acidic OER, while further increasing their mass activity and durability is still a significant challenge towards realizing their practical application in PEMWEs.[3]

At present, nanostructure engineering is one of the most efficient strategies to improve the catalyst performance by increasing active sites,[4] enhancing intrinsic activity,[5] and/or improving catalysts' structural stability.[6] However, nanomaterials easily undergo agglomeration, which severely decrease the exposure of active sites. Generally, anchoring nanostructured active species on carbonaceous substrates is a commonly used method to impede the agglomeration. However, typical carbon-based materials show unsatisfactory electrochemical stability and are easily oxidized at high potentials in acidic media.[2] We recently found that the GCN nanosheets exhibit excellent stability at high potentials, substantially superior to typical carbonaceous materials (Figure S1), indicating that the GCN nanosheets can serve as a chemically stable substrate for constructing robust OER electrocatalysts. Herein, a heterostructure engineering strategy was deployed to design IrO_2/GCN heterostructures toward efficient oxygen evolution in acidic medium. In addition to the excellent chemical stability, the C- and particularly N-rich coordination environment of GCN would induce strong electronic interaction and chemical bonding between IrO_2 and GCN, which would modulate the atomic coordination and electronic structure of Ir active sites accordingly.[7] Meanwhile, the superhydrophilicity of GCN nanosheets would endow the heterostructured catalyst with a superhydrophilic surface, promoting the gas desorption process as well.

The IrO_2/GCN heterostructures were synthesized as schematically illustrated in Figure 1a. GCN nanosheets were firstly exfoliated and functionalized, then IrO_2 nanoparticles (NPs) were anchored on GCN nanosheets via a hydrothermal process followed by annealing in air (details in Supporting Information). As shown in Figure 1b, typical diffraction peaks of rutile IrO_2 (JCPDS 15-0870) and GCN (JCPDS 87-1526) are present in the XRD patterns of IrO_2/GCN containing 40 wt% IrO_2 (40-IG).[8] The relative density of the diffraction peak at 28.0° of 40-IG increases significantly compared with IrO_2 due to the merging of the GCN peak at 27.8°. The Fourier-transform infrared spectroscopy (FT-IR) further proves the presence of GCN in 40-IG (Figure S2).[9] The transmission electron microscopy (TEM) images (Figure 1c-d) illustrate that IrO_2 NPs are well dispersed on GCN nanosheets. As revealed by the HRTEM (Figure 1e) and the fast Fourier transform patterns (FFT, Figure 1f), the lattice spacing of 0.26 and 0.31 nm can be assigned to the (101) and (110) planes of IrO_2, respectively. The loading content of IrO_2 can be controlled by altering the precursor ratio. Similar to 40-IG, IrO_2 NPs are well dispersed in 17-IG and 25-IG (Figure S3a-b), while severe agglomeration is shown in 50-IG and bare IrO_2 (Figure S3c-f).

[*] J. Chen[+], G. Zhao[+], Dr. K. Rui, M. Lao, Y. Chen, Prof. S. X. Dou, Dr. W. Sun
Institute for Superconducting and Electronic Materials, Australian Institute for Innovative Materials, University of Wollongong, Wollongong, NSW 2522, Australia
E-mail: wenping@uow.edu.au
Dr. X. Zheng
National Synchrotron Radiation Laboratory University of Science and Technology of China, Hefei, 230029, P. R. China
E-mail: zxs@ustc.edu.cn
Dr. P. Cui[+]
Key Laboratory of Soil Environment and Pollution Remediation, Institute of Soil Science, Chinese Academy of Sciences, Nanjing 210008, P. R. China
Prof. Y. Jiang, Prof. H. Pan
School of Materials Science and Engineering, Zhejiang University, Hangzhou 310027, P. R. China
[+] These authors contributed equally to this work.

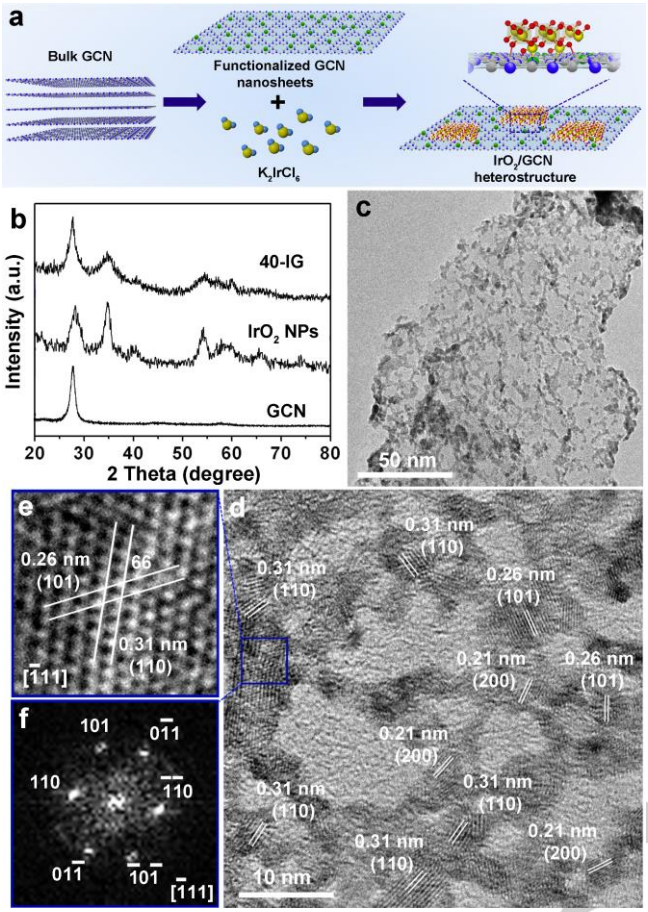

Figure 1. (a) Schematic illustration for synthesizing IrO_2/GCN. (b) XRD patterns of 40-IG, IrO_2 NPs, and GCN. (c) TEM image of 40-IG. (d-e) HRTEM of 40-IG. (f) The corresponding FFT patterns of (e).

The X-ray photoelectron spectroscopy (XPS) survey spectra (Figure S4a) confirms the presence of C, N, Ir, and O elements in 40-IG. Notably, the binding energy of Ir 4f in 40-IG shifts negatively by 0.2 eV, and that of N 1s shifts positively by 0.2 eV as compared with bare IrO_2 NPs and GCN, respectively (Figure 2a-b). Deconvolution of the N 1s XPS spectra indicates the formation of Ir-N bond, demonstrating the strong electronic interaction at the IrO_2/GCN interfaces. Meanwhile, the variations in binding energies indicate that electron transfers from GCN to IrO_2, resulting in a higher electron density around Ir atoms.[10] Moreover, deconvolutions of the high-resolution XPS spectra of C 1s (Figure S4b) reveal that, besides the typical peaks for GCN,[11] two additional peaks are shown in 40-IG that can be assigned to the C-O (285.9 eV) and C=O (288.3 eV) bonds, indicating the formation of oxygen bridges between IrO_2 and GCN.[8b] The formation of C=O bond subsequently results in a positive shift in the binding energies of O 1s (Figure S4c). Furthermore, additional peaks are displayed at around 1710 cm^{-1} in the Raman spectroscopy of 40-IG (Figure S4d), which is a strong evidence for the formation of C=O bond.[12]

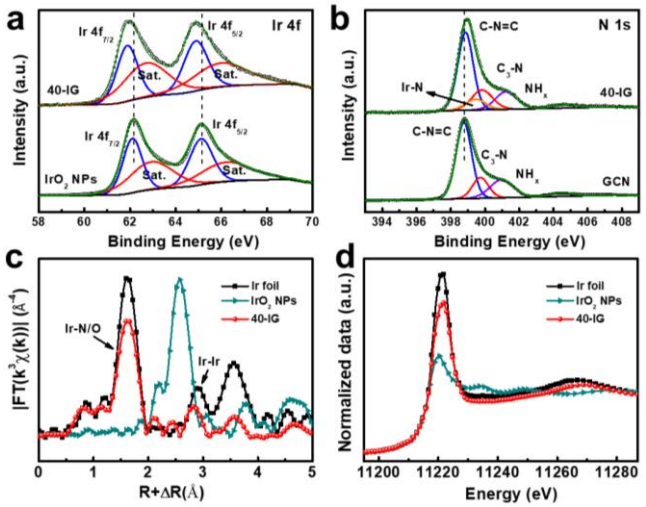

Figure 2. (a) Ir 4f XPS spectra of 40-IG and IrO_2. (b) N 1s XPS spectra of 40-IG and GCN. (c) Fourier transforms of k^3-normalized Ir L_{III}-edge EXAFS of 40-IG, IrO_2 NPs, and Ir foil. (d) The Ir L_{III}-edge XANES spectra for 40-IG, IrO_2 NPs, and Ir foil.

The local atomic coordination environment of Ir atoms is probed by extended X-ray absorption fine structure spectroscopy (EXAFS, Figure 2c), and the quantitative fitting results are listed in Table S1. For 40-IG, owing to the partial substitution of the longer Ir-N bond, the resulted Ir-O/N bond distance (2.00 Å) is a bit longer than Ir-O of bare IrO_2 NPs (1.99 Å).[13] However, Ir-Ir bonds of 40-IG (3.13 and 3.54 Å) are compressed compared with bare IrO_2 NPs (3.16 and 3.59 Å), indicating the formation of distorted IrO_6 octahedrons.[14] Significantly, the compressed Ir-Ir bond can weaken the adsorption of O-intermediates, thus facilitating the rate-determining process for OER.[15] Meanwhile, the decreased coordination numbers of Ir-O and Ir-Ir in 40-IG indicate the existence of abundant low-coordinated Ir sites, which is further proved by the Wavelet transform (WT) analysis of Ir K-edge EXAFS oscillation (Figure S5). Notably, the decreased coordination numbers together with the formation of Ir-N bond increase the electron density at Ir sites, which lower the electrostatic interactions,[16] and hence further weaken the binding of O-intermediates. Figure 2d shows the Ir L_{III}-edge of X-ray absorption near edge structures (XANES) spectra. The apparent decline in the white-line peak intensity of 40-IG compared with IrO_2 NPs indicates an increased occupation of 5d state for 40-IG, leading to a variaiton in 5d electron orbital which subsequently modulate the binding energy between Ir and O-intermediates.[14, 15b] Therefore, the modulated atomic coordination environment and the tuned electronic structures lead to a weaker binding between IrO_2 and O-intermediates, thus promoting the rate-determining step of OER occurring on the surface of IrO_2.

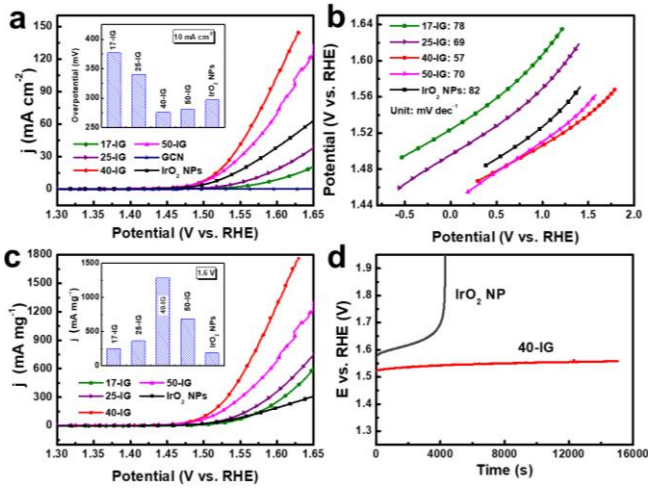

Figure 3. (a) LSV polarization curves measured at a scan rate of 5 mV s^{-1} (Inset: overpotential at 10 mA cm^{-2}). (b) Tafel plots derived from LSV curves. (c) LSV curves plotted based on IrO_2 mass-normalized current density (Inset: current densities at 1.6 V). (d) Chronopotentiometry of IrO_2 NPs and 40-IG at a current density of 20 mA cm^{-2}.

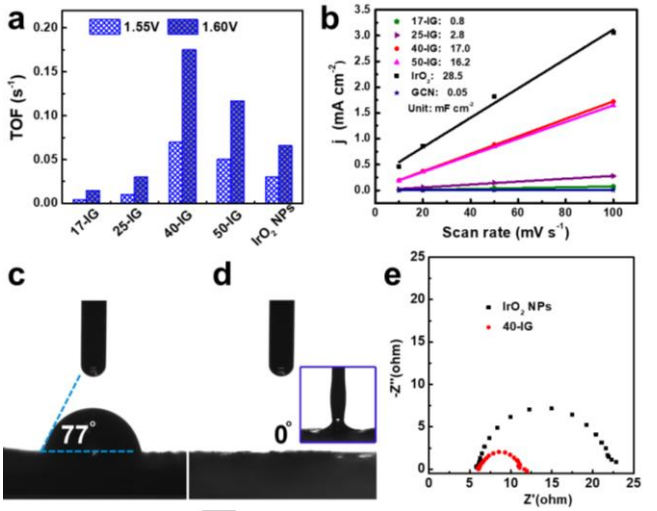

Figure 4. (a) TOF values at 1.55 and 1.6 V, respectively. (b) The current density difference at 1.35 V plotted against scan rate. (c-d) Contact angle measurements of IrO_2 NPs and 40-IG, respectively. The inset image in (d) demonstrates the superhydrophicility of 40-IG. (e) Electrochemical impedance spectroscopy (EIS) of 40-IG and IrO_2 NPs measured at 1.6 V.

The electrochemical test was then carried out to evaluate the catalytic performance of the samples, and all potentials are reported versus reverse hydrogen electrode (RHE) with 95% iR-correction. As shown in Figure 3a, 40-IG delivers the highest catalytic activity with an overpotential of 276 mV at 10 mA cm^{-2} in 0.5 M H_2SO_4. Meanwhile, the Tafel slope is decreased from 82 mV dec^{-1} for IrO_2 NPs to 57 mV dec^{-1} for 40-IG, demonstrating the improved OER kinetics on the IrO_2/GCN heterostructures (Figure 3b). Notably, all the IrO_2/GCN heterostructures show dramatically enhanced mass activity (Figure 3c), indicating that the presence of GCN nanosheets is critical for accelerating the oxygen evolution kinetics on IrO_2. In particular, 40-IG exhibits extremely high mass activity of 1280 mA mg^{-1} at 1.6 V, which is by far the highest mass activity among the reported IrO_2-based catalysts under similar testing conditions (Table S2). More significantly, as shown in Figure 3d, IrO_2 quickly loses its activity within 1.2 h due to the dissolution of active sites at high potentials,[17] while the potential of 40-IG increases by only 35 mV after 4-h chronopotentiometry test at 20 mA cm^{-2}, demonstrating the substantially improved durability under acidic OER condition for 40-IG.

Several synergistic factors are responsible for the significant performance improvement of the IrO_2/GCN heterostructures. Firstly, the strong interaction between IrO_2 and the substrate modulates the atomic coordinations and electronic structures at Ir sites, leading to the formation of the compressed Ir-Ir bond in IrO_2/GCN. This compressive Ir-Ir bond can effectively tune the Ir 5d orbitals and thus weaken the rate-determining O-intermediates adsorption process,[14, 15b, 15c] which lowers the reaction barrier for the formation of HOO* and improves the intrinsic activity.[18] As revealed in Figure 4a and Figure S6, 40-IG exhibits much larger TOF values than bare IrO_2 NPs, confirming the substantially enhanced intrinsic activity.

Secondly, the unique architecture of the heterostructured catalyst ensures a high exposure of active sites. The double-layer capacitance (C_{DL}) determined from CVs (Figure S7) was deployed to evaluate the electrochemically active surface area (ECSA) of the samples. The C_{DL} is 28.5 and 17.0 mF cm^{-2} for pure IrO_2 and 40-IG, respectively (Figure 4b), which means that 40-IG containing 40 wt% IrO_2 accounts for 60% of C_{DL} for pure IrO_2. The greatly increased exposure of active sites can be ascribed to the confinement effect of GCN substrate induced by the strong chemical binding between GCN and IrO_2.

Thirdly, the superhydrophilic GCN nanosheets endow the heterostructured catalyst system a superhydrophilic surface, which is critical for the electrolyte penetration and gas adsorption/desorption kinetics.[19] According to the static contact angle measurements (Figure 4c-d and Video S1-S3),[20] 40-IG becomes superhydrophilic with a contact angle of 0° after introducing the superhydrophilic GCN nanosheets (Figure S8). The superhydrophilicity of 40-IG would substantially facilitate OER kinetics. Moreover, a physical mixed IrO_2-GCN sample also exhibits improved hydrophilicity (Figure S9) and enhanced catalytic activity than bare IrO_2 (Figure S10), further verifying the significance of hydrophilicity for faster oxygen evolution. Figure 4e shows 40-IG has a significantly lower reaction resistance (6.4 Ω) than bare IrO_2 (20 Ω), illustrating accelerated charge transfer and mass diffusion processes at the 40-IG electrode/electrolyte interface, which is closely associated with the highly dispersed active sites and superhydrophilicity of the heterostructured catalysts.

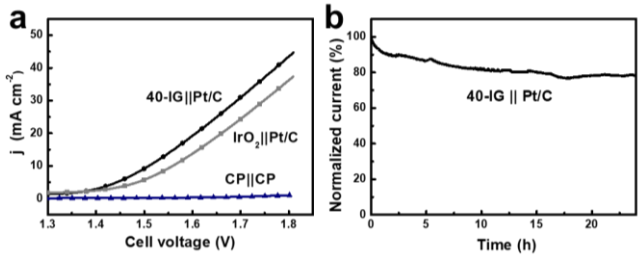

Figure 5. (a) LSV curves of the water splitting devices at a scan rate of 5 mV s^{-1}. (b) Chronoamperometric measurement of the 40-IG||Pt-C full cell at 1.6 V.

Fourthly, the highly stable GCN substrate is beneficial to achieving high structural stability. The TEM image of 40-IG after durability test reveals that the heterostructure morphology is well preserved (Figure S11), demonstrating the excellent structural stability of 40-IG. It can be inferred that the strong chemical bonding at the IrO_2/GCN heterostructure interface inhibits the aggregation and corrosion of IrO_2 during the electrocatalysis process in acidic medium, thereby maintaining high structural integrity and improving the durability.

In order to further evaluate the potential of applying 40-IG in practice, a full water splitting device with 40-IG as the anode and the commercial 20% Pt/C as the cathode was assembled (40-IG||Pt/C, Figure S12). A low voltage of 1.51 V is required to deliver 10 mA cm^{-2} for the 40-IG||Pt-C full cell (Figure 5a), which is superior to the IrO_2||Pt/C cell with bare IrO_2 as the anode (1.56 V to reach 10 mA cm^{-2}). Impressively, the performance of the overall water splitting device is by far the best among the cells with noble metal-based electrocatalysts under similar testing conditions (Table S3). The full cell is capable of producing hydrogen rapidly driven by a single 1.5-V battery (Video S4). Very interestingly, we find that the O_2 bubbles on the 40-IG electrode are much smaller and desorb more quickly than those on the bare IrO_2 electrode (Video S5 and S6). These results can be attributed to the superhydrophilicity of 40-IG as discussed previously, and the rapid O_2 desorption behavior is particularly vital at high operating voltages.[19] As shown in Figure 5b, the 40-IG||Pt-C full cell also exhibits excellent durability with high current retention of 78.5 % after operating at 1.6 V for 24 h. These results clearly demonstrate that IrO_2/GCN heterostructures possess great potential toward developing high-performance and durable water splitting devices.

In summary, new IrO_2/GCN heterostructures with IrO_2 NPs confined on superhydrophilic and highly stable GCN nanosheets are developed toward accelerated oxygen evolution kinetics for efficient water splitting. The unique C- and particularly N-rich coordination environment of GCN induces strong interaction between IrO_2 and GCN, which eventually modulates the electronic structure of Ir active sites with low coordination number. Meanwhile, the multifunctional GCN nanosheets endow the heterostructured catalyst system with a superhydrophilic surface and abundant stable active sites. This work not only demonstrates the feasibility of combining all the favorable characters in one catalyst system by the heterostructure engineering strategy, but also provides new insights into the rational design and development of efficient electrocatalysts for a variety of applications.

Acknowledgments

This work was financially supported by the Australian Research Council (ARC) DECRA Grant (DE160100596) and AIIM FOR GOLD Grant (2018, 2019). This work was also partially supported by National Natural Science Foundation of China (Grant no. 11875258, 11505187 and 41701359). The authors acknowledge use of facilities within the UOW Electron Microscopy Centre and the staff of beamline BL14W1 at Shanghai Synchrotron Radiation Facility for their support in XAFS measurements.

Keywords: heterostructure • graphitic carbon nitride • iridium oxide • oxygen evolution reaction • electrocatalysis

[1] a) J. A. Turner, *Science* **2004**, *305*, 972-974; b) K. Rui, G. Zhao, Y. Chen, Y. Lin, Q. Zhou, J. Chen, J. Zhu, W. Sun, W. Huang, S. X. Dou, *Adv. Funct. Mater.* **2018**, *28*, 1801554.

[2] M. Carmo, D. L. Fritz, J. Mergel, D. Stolten, *Int. J. Hydrogen Energy* **2013**, *38*, 4901-4934.

[3] a) R. Tobias, N. H. Nhan, T. Detre, S. Robert, S. Peter, *Adv. Energy Mater.* **2017**, *7*, 1601275; b) J. Mahmood, M. A. R. Anjum, S.-H. Shin, I. Ahmad, H.-J. Noh, S.-J. Kim, H. Y. Jeong, J. S. Lee, J.-B. Baek, *Adv. Mater.* **2018**, *30*, 1805606.

[4] a) A.-L. Wang, H. Xu, G.-R. Li, *ACS Energy Lett.* **2016**, *1*, 445-453; b) T. Ling, D.-Y. Yan, Y. Jiao, H. Wang, Y. Zheng, X. Zheng, J. Mao, X.-W. Du, Z. Hu, M. Jaroniec, S.-Z. Qiao, *Nat. Commun* **2016**, *7*, 12876; c) J. Wang, H.-x. Zhong, Z.-l. Wang, F.-l. Meng, X.-b. Zhang, *ACS Nano* **2016**, *10*, 2342-2348; d) Z. Dai, H. Geng, J. Wang, Y. Luo, B. Li, Y. Zong, J. Yang, Y. Guo, Y. Zheng, X. Wang, Q. Yan, *ACS Nano* **2017**, *11*, 11031-11040.

[5] a) I. C. Man, H.-Y. Su, F. Calle-Vallejo, H. A. Hansen, J. I. Martínez, N. G. Inoglu, J. Kitchin, T. F. Jaramillo, J. K. Nørskov, J. Rossmeisl, *ChemCatChem* **2011**, *3*, 1159-1165; b) G. Zhao, K. Rui, S. X. Dou, W. Sun, *Adv. Funct. Mater.* **2018**, *28*, 1803291; c) Y. Zhang, Q. Zhou, J. Zhu, Q. Yan, S. X. Dou, W. Sun, *Adv. Funct. Mater.* **2017**, *27*, 1702317.

[6] a) J. Li, G. Chen, Y. Zhu, Z. Liang, A. Pei, C.-L. Wu, H. Wang, H. R. Lee, K. Liu, S. Chu, Y. Cui, *Nat. Catal.* **2018**, *1*, 592-600; b) Q. Zhou, Y. Chen, G. Zhao, Y. Lin, Z. Yu, X. Xu, X. Wang, H. K. Liu, W. Sun, S. X. Dou, *ACS Catal.* **2018**, *8*, 5382-5390.

[7] a) K. Yuan, C. Lu, S. Sfaelou, X. Liao, X. Zhuang, Y. Chen, U. Scherf, X. Feng, *Nano Energy* **2019**, *59*, 207-215; b) C.-Y. Su, H. Cheng, W. Li, Z.-Q. Liu, N. Li, Z. Hou, F.-Q. Bai, H.-X. Zhang, T.-Y. Ma, *Adv. Energy Mater.* **2017**, *7*, 1602420.

[8] a) J. Lim, D. Park, S. S. Jeon, C. W. Roh, J. Choi, D. Yoon, M. Park, H. Jung, H. Lee, *Adv. Funct. Mater.* **2018**, *28*, 1704796; b) Y. Chen, Q. Zhou, G. Zhao, Z. Yu, X. Wang, S. X. Dou, W. Sun, *Adv. Funct. Mater.* **2018**, *28*, 1705583.

[9] H.-x. Zhong, Q. Zhang, J. Wang, X.-b. Zhang, X.-l. Wei, Z.-j. Wu, K. Li, F.-l. Meng, D. Bao, J.-m. Yan, *ACS Catal.* **2018**, *8*, 3965-3970.

[10] a) Y. Peng, B. Lu, L. Chen, N. Wang, J. E. Lu, Y. Ping, S. Chen, *J. Mater. Chem. A* **2017**, *5*, 18261-18269; b) C.

Kwangrok, L. Seungjun, S. Yeonjun, O. Junghoon, K. Sujin, P. Sungjin, *2D Mater.* **2015**, *2*, 034019.

[11] a) S. Zhang, L. Gao, D. Fan, X. Lv, Y. Li, Z. Yan, *Chem. Phys. Lett.* **2017**, *672*, 26-30; b) C. Pu, J. Wan, E. Liu, Y. Yin, J. Li, Y. Ma, J. Fan, X. Hu, *Appl. Surf. Sci.* **2017**, *399*, 139-150.

[12] B. Grabowska, M. Sitarz, E. Olejnik, K. Kaczmarska, B. Tyliszczak, *Spectrochim. Acta A* **2015**, *151*, 27-33.

[13] a) X.-N. Li, Z.-J. Wu, H.-J. Zhang, X.-J. Liu, L. Zhou, Z.-F. Li, Z.-J. Si, *Phys. Chem. Chem. Phys.* **2009**, *11*, 6051-6059; b) H. Junge, N. Marquet, A. Kammer, S. Denurra, M. Bauer, S. Wohlrab, F. Gärtner, M.-M. Pohl, A. Spannenberg, S. Gladiali, M. Beller, *Chem.-Eur. J.* **2012**, *18*, 12749-12758.

[14] W. Sun, Y. Song, X.-Q. Gong, L.-m. Cao, J. Yang, *Chem. Sci.* **2015**, *6*, 4993-4999.

[15] a) W. Sun, Z. Wang, W. Q. Zaman, Z. Zhou, L. Cao, X.-Q. Gong, J. Yang, *Chem. Commun.* **2018**, *54*, 996-999; b) J. R. Petrie, V. R. Cooper, J. W. Freeland, T. L. Meyer, Z. Zhang, D. A. Lutterman, H. N. Lee, *J. Am. Chem. Soc.* **2016**, *138*, 2488-2491; c) D.-Y. Kuo, C. J. Eom, J. K. Kawasaki, G. Petretto, J. N. Nelson, G. Hautier, E. J. Crumlin, K. M. Shen, D. G. Schlom, J. Suntivich, *J. Phys. Chem. C* **2018**, *122*, 4359-4364.

[16] F. Sen, A. Kinaci, B. Narayanan, S. Gray, M. Davis, S. Sankaranarayanan, M. Chan, *J. Mater. Chem. A* **2015**, *3*, 18970-18982.

[17] a) P. Jovanovič, N. Hodnik, F. Ruiz-Zepeda, I. Arčon, B. Jozinović, M. Zorko, M. Bele, M. Šala, V. S. Šelih, S. Hočevar, *J. Am. Chem. Soc.* **2017**, *139*, 12837-12846; b) S. Cherevko, S. Geiger, O. Kasian, A. Mingers, K. J. Mayrhofer, *J. Electroanal. Chem.* **2016**, *774*, 102-110.

[18] J. Feng, F. Lv, W. Zhang, P. Li, K. Wang, C. Yang, B. Wang, Y. Yang, J. Zhou, F. Lin, G.-C. Wang, S. Guo, *Adv. Mater.* **2017**, *29*, 1703798.

[19] W. Xu, Z. Lu, X. Sun, L. Jiang, X. Duan, *Acc. Chem. Res.* **2018**, *51*, 1590-1598.

[20] L. Wang, K. A. Stoerzinger, L. Chang, X. Yin, Y. Li, C. S. Tang, E. Jia, M. E. Bowden, Z. Yang, A. Abdelsamie, L. You, R. Guo, J. Chen, A. Rusydi, J. Wang, S. A. Chambers, Y. Du, *ACS Appl. Mater. Interfaces* **2019**, *11*, 12941-12947.

Entry for the Table of Contents

COMMUNICATION

Iridium oxide/graphitic carbon nitride (IrO_2/GCN) heterostructures with abundant low-coordinated Ir sites and superhydrophilic surfaces are designed toward fast and durable oxygen evolution. The results present an effective GCN-based heterostructure engineering strategy for developing highly active electrocatalysts.

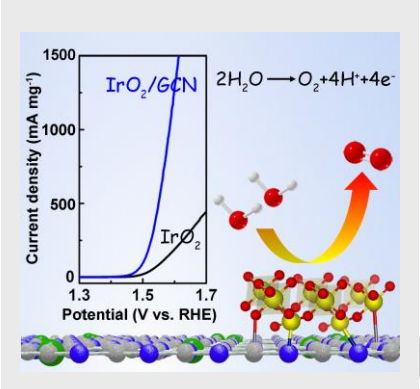

Jiayi Chen[+], Peixin Cui[+], Guoqiang Zhao[+], Kun Rui, Mengmeng Lao, Yaping Chen, Xusheng Zheng, Yinzhu Jiang, Hongge Pan, Shi Xue Dou, and Wenping Sun**

Page No. – Page No.

Low-Coordinated Iridium Oxide Confined on Graphitic Carbon Nitride for Highly Efficient Oxygen Evolution